Journal of Electronic Materials ,DOI: 10.1007/s11664-015-3799-0, May 2015.

Modification of chemically exfoliated graphene to form efficient piezoresistive polystyrene-graphene composites

Farzad Nasirpouri[1,*], *Hassan Pourmahmoudi*[1], *Farhang Abbasi*[2], *Samuel Littlejohn*[3], *Ashok S. Chauhan*[3], *Alain Nogaret*[3]

[1] *Faculty of Materials Engineering, Sahand University of Technology, Tabriz 51335-1996, Iran*

[2] *Faculty of Polymer Engineering, Sahand University of Technology, Tabriz, Iran*

[3] *Department of Physics, University of Bath, Bath BA2 7AY, UK.*

Abstract

We report on the chemical exfoliation of graphene oxide from graphite and its subsequent reduction into graphene nanosheets (GNs) to obtain highly conductive composites of graphene sheets in a polymer matrix. The effect of using either graphite nanoparticles or flakes as precursors as well as different drying methods was investigated to obtain multilayer graphene sheets of atomically controlled thickness which was essential to optimizing their dispersion in polystyrene (PS) polymer matrix. In-situ emulsion polymerization of the styrene monomer in the presence of GN was performed to obtain thin composite films which had a highly uniform dispersion and smaller numbers of graphene layers when GNs were reduced from flake graphite with freeze drying. The highest electrical conductivity in the PS-GN composites was found to be ~0.01 S/m for a graphene filling fraction of 2%. The piezoresistance of the PS-GN composites was evaluated and used in pressure sensor arrays which demonstrated pressure field imaging capability.

Keywords: Graphene, chemical exfoliation, polystyrene, Raman spectroscopy.

*-*Corresponding author: Tel: +98 411 3459450, Fax: +98 4113444333, Email:* nasirpouri@sut.ac.ir *or* f_nasirpouri@yahoo.com (F. Nasirpouri)

1- Introduction

Since its discovery by A. Geim and K. S. Novoselov in 2004 [1], graphene has been the source of many scientific breakthroughs and promises important applications in nanotechnology [2-4]. Graphene derives from the sp^2 hybridization of tetravalent carbon atoms which creates a two dimensional (2D) honeycomb network of carbon atoms. The fourth π-orbital is out of the graphene plane and binds to other planes via van der Waals interactions to form graphite [3]. The amazing properties of this material include very high mechanical strength, high mobility at room temperature and exotic electronic properties underpinned by its relativistic energy spectrum, van Hove singularities in the optical spectrum and negative permittivity in the THz spectrum leading to important applications in electronics, optics and plasmonics [4].

Among various methods for preparing graphene, the chemical reduction of graphite into graphene oxide (GO), known as the Hummer's method, has been frequently used [5]. In this method, GO is generally produced by oxidation of highly oriented pyrolytic graphite (HOPG) under the action of strong oxidants like potassium permanganate mixed with concentrated sulfuric acid, followed by sonication [6]. This results in heavily oxygenated, hydroxyl and epoxide functional bearing groups forming on graphite basal planes. In addition, carbonyl and carboxyl groups form near the sheet edges [7-8]. The formation of C-O covalent bonds converts sp^2-hybridized carbon atoms into sp^3 [5-10]. Coulomb repulsion between electro-negatively charged oxygen atoms increases the interlayer distance. This enables the oxidized graphite to be easily exfoliated into individually dispersed single layers by sonication in water. Because of the destruction of the sp^2 bonds, the conductivity GO ($\sim 10^{-4}$ S/m) is typically 10^6 times smaller than that of graphene ($\sim 10^2$ S/m) [11]. GO can be subsequently reduced to graphene nanosheets (GNs) via hydrazination [12]. Graphene is an important

component of composites used in nanoelectromechanical systems (NEMS) [13], sensors [14] and flexible electronics [15,16]. A major challenge however, is to disperse the atomically thin GO nanosheets (GONs) in the polymeric matrix. To this end, several groups [17-21] have functionalized GONs with isocyanate groups [22] that serve as precursors to polymerization [23]. The isocyanate treatment reduces the hydrophilic character of GONs by forming amide and carbamate ester bonds to the carboxyl and hydroxyl groups of GO, respectively. As a result, the isocyanate-modified GO no longer exfoliates in water but readily forms stable dispersions in polar aprotic solvents (such as N,N-dimethylformamide (DMF)). The latter dispersions consist of completely exfoliated, functionalized individual GO sheets which are readily miscible in organic polymers, hence facilitating synthesis of graphene–polymer composites [24, 25]. Octadecylamine is an alternative functionalizing agent [24]. Post-exfoliation, the GONs may be reduced to graphene and functionalized with monomers and pre-polymers [26-28] to obtain electrically conductive composite materials. In situ polymerization is a very efficient method to uniformly disperse chemically reduced graphene and bind the filler to the polymer matrix [29].

This work reports a comprehensive investigation of the first stages of the chemical synthesis of GONs from graphite to GN-polymer devices. The resulting GNs were used to obtain composites having the highest electrical conductivity achieved. They have been realised by applying a multi-step procedure to synthesize GONs by a modified Hummer method from different types of graphite, through exfoliation and reduction of GONs to GNs and their successful incorporation in polymer based composites. We have polymerized the styrene monomer in the presence of chemically reduced GNs to prepare graphene-polystyrene composites. We have investigated the electrical conductivity and piezoresistance of chemically reduced GN-polystyrene composites synthesized under optimum conditions including initial graphite precursor, vacuum and freeze drying and in-situ emulsion

polymerization. The structure of the graphene multilayers reduced by different methods was examined using X-ray diffraction, Raman spectroscopy, scanning electron microscopy (SEM), Fourier transform infrared spectroscopy (FTIR) to compare the effect of different synthesis methods on the electrical conductivity of the composite films. The dependence on the graphene filling fraction and graphene reduction method was also investigated. The graphene/polystyrene composites were molded in the shape of piezoresistive sensing arrays used for imaging pressure.

2- Experimental

2-1 Preparation of graphene-oxide nanosheets (GONs)

In this study we used two forms of graphite including particles (Sigma-Aldrich, product no. 496588, particles size <150 μm) and flakes (Sigma-Aldrich, product no. 332461, size ~150 μm). Hummer's method in its primary and modified forms was employed to oxidize graphite [5, 30]. Following Hummer's procedure, we have mixed 2 g of graphite (flake and particle), 1 g $NaNO_3$ and 46 ml sulfuric acid (98%) in a solution which we then stirred in a 500 ml flask in an ice bath (0°C). Potassium permanganate ($KMnO_4$-99%) (6 g) was then added slowly to the suspension to prevent the temperature from rising above 20°C. The reaction mixture was then cooled to 2°C and the mixture was stirred for 1 h. Then it was removed from the ice bath and stirred again at 35°C for 30 min. Distilled water (92 ml) was slowly added to the reaction vessel over a period of 20 min to keep the temperature under 98°C. It was further diluted by adding 280 ml distilled water during an additional 20 min, before adding 10 ml hydrogen peroxide (H_2O_2- 30%) for 30 min in order to further oxidize the graphite and remove excess permanganate ions. The mixture was left to rest overnight. GO colloids were separated from the liquid by centrifugation followed by decantation. In order to achieve full neutrality in the solid sediment, it was washed five times over with distilled water, and was centrifuged again. In order to achieve optimum GO, we dried the suspension

first in an oven at 55°C for 12 h and , after the centrifugating step, allowed the powder to settle for 24 h in a vacuum dryer (0.3 mbar at 65°C) until a brownish solid powder was obtained, (Fig 1a,b). The brownish color of the suspension obtained according to the primary Hummer's procedure indicates that the oxidation reaction is only partially complete as residual amounts of initial material remain non-oxidized (cf. Figure 1a). This will be further discussed in the Results section. We prepared additional samples using a *modified Hummer* method in which a stronger oxidizing agent was employed. This consisted of 30 ml hydrogen peroxide (H_2O_2- 35%), (cf. 10 ml of H_2O_2- 30% in the primary method). However, after each step, the solution was aged for 24 h before centrifugation to decant the solution (Figure 1b). After this procedure, a black powder was obtained (Figure 1c).

2-2 Reduction of graphene oxide to graphene

The next step was the exfoliation of GONs by sonication and then reduction reaction to achieve GNs. 500 mg of GO particles synthesized by the Hummer and modified Hummer methods were dispersed in 100 ml of deionized water in a 250 ml flask with assistance of ultrasonic bath at a power of 100 W for 30 min, followed by 150 W for 30 min and 100 W for 30 min. The resulting solution contained GONs which were reduced to GN in the next step. The reduction of GO solution was carried out by adding 100 ml hydrazine hydrate 99% purity at a temperature of 100°C for 24 h. To prevent agglomeration in this step, we added triethanolamine: TEA-$N(CH_2CH_2OH)_3$ as the stabilizer. GNs were separated from the liquid by centrifugation followed by decantation. In order to remove the stabilizers, the sediment was washed five times over with distilled water and methanol, and was then centrifuged again. Two methods for drying GN were employed including vacuum drying for 24 h in a vacuum dryer (0.3 mbar at 65°C) and freeze drying. Table I lists the GN samples prepared according to various methods.

2-3 Preparation of GN-polystyrene composites

In-situ emulsion polymerization was used to prepare PS-GN composites with different GNs contents. In the first step, GNs with different weight percentage were dispersed in 100 ml of distilled water. 10 g styrene monomer was then added to the solution in the presence of sodium dodecylbenzene sulfonate (DBSNa-$C_{12}H_{25}C_6H_4SO_3Na$) as surfactant and potassium persulphate (KSP-$K_2S_2O_8$). KSP starts the polymerization of styrene by dissociation in water, producing radicals, which react with the monomers for polymerization. DBSNa acts as surfactant to stabilize micelles in which KSP radicals and monomers are present and the polymerization takes place. The mixture was stirred in an ultrasonic bath at 50 W for 15 min and then in a magnetic stirrer at a temperature of 80^{o}C until the completion of polymerization reaction. Finally, the powder was separated by adding 1N (*normal*) sulfuric acid to the reactor. Sulfuric acid was used to discharge the ionic parts of DBSNa to stabilize the solid composites. The solution was aged for 6 to 8 h until the complete sedimentation of suspended particles when the solution becomes bright and clear. The powder was then vacuum-dried to form PS-GN composites. The powder composite was hot pressed into discs (1.5 cm in diameter and 2 mm thickness) at 110^{o}C under load of 150 bar. Table II summarizes the PS-GN composites prepared in this study. The weight percentage ratio of GN/polymer was chosen in a range of up to 2%, as this amount of graphene filler has been shown to demonstrate the highest possible conductivity [18].

2-4 Characterization of GO, GN and GN/PS

Crystallographic structure of materials was examined by X-ray Diffraction (XRD- Brukers AXS D8 Avance) using Cu $_{(K\alpha)}$. Raman spectroscopy (model: almega thermo nicolet dispersive Raman spectrometer) was used to study the graphene structures with wave number

ranging 100-4200 cm^{-1}, wave length of 532 nm and resolution of 4 cm^{-1} and laser beam power of 100 mW. Fourier transform infrared spectroscopy (FTIR-model: UNICAM) was used with wave number ranging 400-4000 cm^{-1} to probe molecular structure properties. Scanning electron microscopy (SEM, model: field emission Hitachi S4160) was used to study the morphology of the materials. A house-made four-probe set-up was used to measure the electrical conductivity of composites.

3- Result and discussion

3-1) GON and GN

XRD patterns of pristine graphite, as-synthesized GON, and GN are shown in Figure 2. Graphite powder and flakes exhibit almost the same XRD spectra. The XRD pattern of raw graphite sample reveals a very sharp and intense (002) Bragg peak at 2θ =26.5˚ and a (004) Bragg peak at 2θ=54.5˚ (Figure 2a). We find that the Hummer and modified Hummer method produce differences in GON structure. Graphite oxides resulting from the primary Hummer's method (Figure 2b) exhibit a diffraction peak at 2θ=12.1˚ which has negligible intensity and corresponds to graphite oxide nanosheets in agreement with previous reports [31,32]. However, the (002) main peak of the initial graphite still remains. In contrast, the modified Hummer's method (Figure 2c) gives a broad diffraction peak with high intensity at 2θ=12.1˚ . The lower index graphite Bragg peak at 2θ=26.62^{o} were completely eliminated, and the only main (001) Bragg peak arises from graphite oxide diffraction indicating of a complete oxidation process and the formation of GON. These findings indicate the formation of single layer graphene oxide. As is shown in Figure 1a, the sample oxidized by the primary Hummer's method exhibits a brownish color, achieved during the oxidization of graphite. The color is lighted due to the incomplete reduction of permanganate ions. Using the modified Hummer's method, its color becomes dark brown (Figure 1b) [33]. The results are

almost the same as those obtained for post-oxidized graphite using the two forms of initial graphite used in this study (Figures 2c, 2d).

We calculated the distance between the graphite (002) planes, defined as d_{002}, using the Bragg formula:

$$\lambda = 2d_{002}\sin\theta \qquad (1)$$

where λ=1.5406 Å , and θ angle. Using the XRD spectra, we obtained d_{002}, 0.34 and 0.72 nm for the graphite and GO nanosheets, as shown in Table III.

In the next stage, we characterize GN reduced from GONs. Figure 3 compares XRD patterns obtained for GN synthesized by different methods and shows SEM images of GN5 and GN7 samples. SEM images show GNs with highly crumpled and overlapped structures in the stack. There is not much difference in the morphology between GNs synthesized by different methods which can be attributed to the rapid removal of functional groups such as hydroxyl bonds during exfoliation. This results in a wrinkled structure, and fluffy physical appearance [34].

This type of morphology is desired for the dispersion of GNs as the wrinkling and crumpling of flat sheets can prevent them from stacking densely [35]. This will be discussed later in PS-GN composites.

XRD patterns of GN samples generally show a very wide peak at 2θ=21.90 to 23.56° depending on the synthesis. It has been previously shown [36] that XRD pattern from fine particle carbon materials with hexagonal structure only shows the three dimensional lattice reflections as (*00l*) and the two dimensional reflections as *(hk)*. Regardless of the strain, the size of crystallite can be estimated from width of the diffraction peaks. The parallel layer dimensional in a hexagonal crystal (*c*-axis) was L_c and can be calculated by the Scherrer equation from the full width at half intensity maximum (FWHM) called β of (002) reflection

[34]:

$$L_c = \frac{0.94\lambda}{\beta cos\theta} \quad (2)$$

The layer dimension (L_a) is planar crystallite size of (001) peak and is obtained from full width at half maximum of the *hk* reflection using the two-dimensional lattice equation:

$$L_a = \frac{1.84\lambda}{\beta\ cos\theta} \quad (3)$$

The values of d_{002}, L_c and L_a for all materials synthesized were calculated and the results are summarized in Table III. A significant increase in the inter-atomic distance takes place due to the incorporation of oxygen and hydroxyl operating groups between the graphite layers and therefore due to the presence of oxygenated operating groups [7-8]. The d_{002} values calculated for GN samples are much less than those for the GONs and are greater than those of the graphite. Such an increase in interlayer spacing for GNs can be ascribed to the relaxation of lattice constant in atomically thin films formed during the chemical reduction in agreement with previous reports [37-40].

We studied the change of dimension through the entire synthesis from graphite to GO and to GN on the basis of the molecular group formed. Figure 4 illustrates FTIR spectra for GO3, GO5 and GN6 and GN9. To avoid repetitive pictures, the FTIR spectra of some samples are omitted here. Groups operating with carbon and oxygen are seen in all materials. The peaks of about 1100, 1205, 1412, 1622 and 3400^{-1} cm are assigned to groups of C-O, C-O-C, O-H, C=C, and C-O-H [32-34]. In powder graphite, we observed that C=C exhibits the most intense peak while C-O-H groups also exist. However, in flake graphite functional groups of C-O, C-O-C, O-H, C=C and C-O-H have almost the same intensity. FTIR spectrum of GO typically reveals that no significant change occurs for C=C peak, while C-O, C-O-C, O-H and particularly C-O-H peaks have slight increase in intensity which can be due to the

incorporation of oxygen and hydrogen group in the interlayer spacing between carbon atoms. Exfoliation and reduction leads to the formation of GN which is evident with a decrease in C-O-H groups (the peak around 3400 cm^{-1}) in FTIR spectra. In addition, C=C group is intensified which is likely due to the reduction of GO to GN. It is interesting that the intensity of the -C-O-H group is lower in flake graphite than in powder graphite.

It is worth noting that according to Warren [36], equation (3) gives more accurate to estimate of the interlayer spacing at larger size carbon particles (L_a > 5 nm). We have complemented XRD analysis with Raman spectroscopy to assess the lattice integrity of the 2D GN and the number of graphene layers it incorporates.

Figure 5 shows typical Raman spectra taken from GNs reduced from GONs by hydrazination. Raman spectroscopy has been extensively used for probing the crystalline structure of graphene which displays well-known peaks associated with characteristic in-plane and out-of-plane vibronic modes: the D band at about 1350 cm^{-1}, the G band at 1580 cm^{-1}, and the G' band at about 2700 cm^{-1}[41-45]. A second-order dispersion of D band, 2D, is also known [22, 41-45]. Provided that the observed G' band is more intense than G band, it can be concluded that there is a maximum of 4 layers of graphene in the material. However, one cannot infer the precise number of layers from Raman spectra if the structure comprises more than 5 layers [41]. Indeed, our GN materials consist of multilayer graphene sheets which may be formed due to the overlapped and crumpled stacks of graphene. Figure 5b shows the Lorentzian fitting plots of D and G bands calculated for different GNs. The samples synthesized from powder graphite GN5 and GN6 dried under different conditions exhibit more intense D band than the G band. However, for GN7 and GN9 synthesized from flake graphite, G band is more intense than the D band. We focused on two important factors, the peak intensity ratio of D band to G band (I_D/I_G), and FWHM of G band (W_G) [46]. Minimum value of I_D/I_G implies a larger two-dimensional layer structure without edge defects, while

minimum value of W_G, means smaller inhomogeneity between the layers [47]. HOPG exhibits the smallest FWHM of G-band (W_G=14 cm^{-1}) and the lowest intensity ratio (I_D/I_G=0). On the other hand, glassy carbon is a typical disordered carbon structure exhibiting larger FWHM of G-band (W_G=58 cm^{-1}) and high intensity ratio (I_D/I_G=1.8). The planar graphene domain size (La) can be estimated from I_D/I_G intensity ratio using *Tuinstra* & *Koenig* model [48]:

$$L_a = C(\lambda)\left(\frac{I_D}{I_G}\right)^{-1} \quad (4)$$

In our experiments, $C(\lambda)$=4.4 nm, as λ=532 nm. Table IV and Figure 6 compare W_G , I_D/I_G and L_a were calculated from to the Raman spectra of different GN samples. The data show that GNs have a size between 3-6 nm and the order of the structures is between HOPG and glassy carbon.

According to the results of Raman spectroscopy, we find higher structural ordering in GNs reduced from flake graphite precursor. It is observed that the width of G band in GNs synthesized from graphite flakes is narrower than that in those obtained from powders. In addition, the D band obtained for GN7 and GN9 (flake graphite as precursor) is more intense than the G band which shows a higher degree of ordering in these GNs. Furthermore, from our observations on the drying properties of graphene, it is seen that GNs obtained from graphite flake have smaller number of layers (I_D/I_G =0.7324) with respect to those obtained from graphite powder (I_D/I_G =0. 8043) as we observed their drying more difficult. Furthermore, the drying technique also has no significant effect on size of GNs (L_a). In Fig 1c, a photograph of freely settled 0.5 g of GN9 shows a very high volume to mass ratio or very low bulk density, representing the non-agglomerating graphene nanosheets.

3-2) GN/PS composites

GN/PS composites were synthesized by in-situ emulsion polymerization of styrene monomer with different weight percentages ranging 0.5-2% of GN5, GN6, GN7 and GN9 graphene nanosheets. Figure 7a shows a typical SEM image of GN5/PS composites produced which shows GNs uniformly dispersed in the matrix. Individual GNs, however, may be folded and overlap despite forming a continuous network. Higher magnification micrographs (inset) show the network of folded and crumpled GNs inside the polymeric matrix separated by the polymer molecules as they are not forming dense stack [35]. The piezoresistance of this material was measured as a function of pressure, as shown in Figure 7b. The resistance of the composite is governed by the formation of a percolation network whose nodes are the graphene nanosheets. Compression has the effect of bringing the graphene sheets closer to one another by increasing the electron tunneling probability across the insulating matrix. This has the effect of increasing the size of the percolating cluster and therefore decreasing the overall resistance as seen in Fig. 7b. Conversely the destruction of percolating pathways causes a decrease in conductivity. The effect of compression is similar to the effect of increasing graphene filling fraction in that both reduce tunneling barrier width. Using the equation: $\sigma_c = \sigma_f[(\phi - \phi_c)]/(1-\phi_c)]^t$, where σ_c is the composite conductivity, σ_f is the filler conductivity, ϕ is the volume fraction of the filler, one can find out the percolation concentration of the composite [17] and *t* is the percolation exponent which depends on the topology of the network. Fitting data to the equation give the parameters *t* and σ_c. We find that the percolation threshold corresponds to a graphene filling fraction of ϕ_c and above this threshold the conductivity is $\sigma_c \propto (\phi - \phi_c)^4$ [16, 24, 29]. This is discussed in details for the current GN/PS samples as follows.

Figure 8 illustrates the variation of resistivity (or conductivity) as a function of weight percentage of GNs (GN5, GN6, GN7 and GN9). As is evident, any addition of GNs to PS reduces the electrical resistivity. Percolation in all samples under this study occurs around

less than $\phi_c \leq 0.5\%$ indicating the formation of an electrical conductive network of graphene inside polymer. GN6/PS and GN7/PS composites show the highest electrical conductivity about 0.01 S/m at a graphene loading of 2%. Previous reports have also mentioned the production of graphene/PS composites with higher electrical conductivity than our records [30,49]. We understand that in our preparation technique, graphene was initially reduced and then added to polymer, while in the other reports with higher electrical conductivity [17, 44] an excellent homogeneous dispersion was achieved with solution phase mixing of exfoliated phenyl isocyanate-treated GO sheets with PS, followed by in situ chemical reduction of GO. Another reason could be the addition of other reagents like incorporation of polylactic acid [49]. Our results also show that graphene nanosheets reduced have folded and crumpled morphology. SEM images shown in Figure 3, wrinkles, folding and overlap of GNs are seen. It also shows the random aggregation of sheets complicates the estimation of single-layer and multi-layer structure and only crumpled sheets with irregular forms are observed. This is a possible reason for a lower absolute electrical conductivity in the composites reported in other studies [30].

3-3) Pressure sensing with arrays of piezoresistive composite elements.

The best pressure and shear stress sensors are currently obtained using electromechanical devices micromachined in either silicon on III-V semiconductors such as GaAs. Dehé et al. [50] have micromachined pressure sensing devices consisting of a thin semiconductor drum membrane with 4 piezoresistors on top of it which measure the deflection of the membrane hence the pressure applied to it. These sensors have a sensitivity of less than 1%/atmosphere. The diameter of the drums can be no smaller than 100μm otherwise the drum deflection would become too small for a meaningful piezoresistance signal. Hence these sensors are limited in size and sensitivity and require expensive micro-fabrication procedures.

Shear stress sensors on the other hand have been obtained using microfabricated floating platforms supported by the substrate via four cantilevers. The deflection of these cantilevers was monitored by four silicon piezoresistors. Shajii et al. [51], Lv et, al. [52] have demonstrated shear stress sensitivity of the order 100kPa. Shear stress sensors were made with a size of several 100 μm.

To improve sensitivity and miniaturization, we have made sensor arrays using small elements of graphene composite. A 8×8 composite sensor array (Figure 9) was molded with a pitch of 0.1 inch, each piezoresistive element was 1.5mm×15mm in section and 0.1mm thick. These elements were individually addressed by a transistor array at the back of the sensor head (Figure 9b). The change in resistance was read by integrating the current passing through each element in a readout cycle. The integrated signal (proprotional to the resistance) was collected by a Labview program via an digital/analogue acquisition card. The display panel in Figure 9a shows the pressure image sensed by the array on two levels. In this particular example a © symbol was applied on the sensor head resulting in white pixels indicating a high pressure. Through this study we have shown that the above materials have a stronger piezoresistance than MEMs, work in a pressure range of 50Pa-500kPa and can in principle be scaled to dimensions smaller than 100μm.

4- Conclusions

We have synthesized graphene nanosheets using a modified Hummer's method which produces higher quality reduced graphene and enables easier polymerization for making conductive polymers. XRD shows that the Hummer's method produces single layer graphene characterized by a single Bragg reflection on the basal plane. Our study shows that few-layer graphene can be produced starting from HOPG flakes followed by freeze drying. The resulting emulsion displays the best dispersion in solvent. However, the GN is generally

folded and crumpled which lowers sheet conductivity of the GN-polymer composites. Composites were prepared through the polymerization of reduced graphene. These were found to have electrical conductivity as high as 0.01 S/m. The composite also have electromechanical properties which we have used in pressure sensing arrays to image pressure patterns.

References

1. A. K. Geim, K. S. Novoselov *Nat. Mater* **6**, 183 (2007).
2. K. S. Novoselov, A. K. Geim, S. V. Morozov, D. Jiang, M. I. Katsnelson, I. Grigorieva, S. V. Dubonos, A.Firsov, *Science* **306**, 666 (2004).
3. K.S. Novoselov, D. Jiang, F. Schedin, T. J. Booth,V. V. Khotkevich, A. K. Morozov, S. V. Geim, *Proc. Natl. Acad. Sci* **102,** 10451 (2005).
4. J. C. Meyer, A. K. Geim, M. I. Katsnelson, K. S. Novoselov, T. J. Booth, S. Roth, *Nature* **446**, 60 (2007).
5. W. S. Hummers, R. E. Ofeman Preparation of graphitic oxide. *J. Am. Chem. Soc.* **80**, 1339 (1958).
6. D. R. Dreyer, S. Park, C. W. Bielawski, R.S. Ruoff, *Chem. Soc. Rev.* **39**, 228 (2010).
7. H. He, J. Klinowski, M. Forster, A. Lerf, *Chem. Phys. Lett.* **287,** 53 (1998).
8. A.Lerf, H. He, M. Forster, I. J. Klinowski, J. *Phys. Chem. B* **102,** 4477 (1998).
9. W. W Cai1, R. D. Piner, F.J. Stadermann, S. Park, M.A. Shaibat, Y. Ishii,D. Yang, A. Velamakanni, S Jin An, M Stoller, J An, D Chen, R. S. Ruoff, *Science* **26,** 1815 (2008).
10. W. Gao, L. B. Alemany, L. Ci, P.M. Ajayan, *Nature Chem.*, **1.** 403 (2009).
11. Z. Xu, C. Gao, *Macromolecules* **43,** 6716 (2010).
12. V. C. Tung, M. J. Allen, Y. Yang, R. B. Kaner , *Nature Nanotechnology* **4,** 25 (2009).
13. A.D. Smith, F. Niklaus, A. Paussa, S. Vaziri, A.V. Fisher, M. Sterner, F. Forsberg, A. Delin, D. Esseni, P. Palestri, M. Ostling, M.C. Lemme, *Nano lett.* **13**, 3237 (2013).
14. S. Littlejohn, A. Nogaret, G.M. Prentice, G.D. Pantoş, *Adv. Func. Mat.* **23**, 5398 (2013).
15. L.G.P. Martins, Y. Song, T.Y. Zeng, M.S. Dresselhaus, J. Kong, P.T. Araujo, *Proc. Nat. Acad. Sci.* **110**, 17762 (2013).

16. T. Georgiou, R. Jalil, B.D. Belle, L. Britnell, R.V. Gorbatchev, S.V. Morozov, Y.J. Kim, A. Gholinia, S.J. Haigh, O. Makarovsky, L. Eaves, L.A. Ponomarenko, A.K. Geim, K.S. Novoselov, A. Mishchenko, *Nature Nanotech*. **8**, 100 (2013).
17. C. Gomez-Navarro, J C. Meyer, R S. Sundaram, A. Chuvilin, S. Kurasch, M. Burghard, K. Kern, U. Kaiser, *Nano Lett.* **10,** 1144 (2010*)*.
18. S. Stankovich, D. A. Dikin, G. H. B. Dommett, K. M. Kohlhaas, E. J. Zimney, E. A. Stach, R. D. Piner, S. T. Nguyen, R. S. Ruoff, *Nature* **442**, 282 (2006).
19. T. Ramanathan, A. A. Abdala, S. Stankovich, D. A. Dikin, M. Herrera-Alonso, R. D. Piner, D. H. Adamson, H. C. Schniepp, X. Chen, R. S. Ruoff, S. T. Nguyen, I. A. Aksay, R. K. Prudhomme, L. C. Brinson, *Nat. Nanotechnol*. **3**, 327 (2008).
20. S. Ansari, A. Kelarakis, L. Estevez, E P. Giannelis, *Small* **6,** 205 (2010).
21. H. Hu, X. Wang., J. Wang, L. Wan, F. Liu, H. Zheng, R. Chen, C. Xu, *Chemical Physics Letters* **484,** 247 (2010).
22. S. Stankovich, R. D. T. Piner, S. B. Nguyen, R. S. Ruoff, *Carbon*, **44**, 3342 (2006).
23. A.K. Appel, R. Thomann, R. Mulhaupt, *Macromolecular Rapid Comm.* **34**, 1249 (2013).
24. S Littlejohn, A Nogaret, S Crampin, *Advanced Materials*, **23**, 2815 (2011).
25. W. Li, X-Z Tang, H-B Zhang, Z-G Jiang, Z-Z Yu, X-S Du, Y-W Mai, Carbon, **49**, 4724 (2011).
26. G Eda, M Chhowalla, *Nano Lett.*, **9,** 814 (2009).
27. A.V. Raghu, Y.R. Lee, H.M. Jeong, C.M. Shin, *Macromol. Chem. Phys.* **209,** 2487 (2008).
28. A.P. Yu, P. Ramesh, M.E. Itkis, E. Bekyarova, R.C. Haddon, *J. Phys. Chem. C* **111,** 7565 (2007).
29. J Du, H-M Cheng, *Macromol. Chem. Phys.* **213**, 1060 (2012).
30. S. Park, R. S. Ruof, *Nature Nanotechnology* **4,** 217 (2009).
31. L. Zhang, J. Liang, Y. Huang, Y Ma, Y Wang, Y Chen *Carbon* **47**, 3365 (2009).
32. Y. Geng, S. Wang, J.K. Kim, *Journal of Colloid and Interface Science*, **336,** 592 (2009).
33. E. Brauer, Handbook of Preparative Inorganic chemistry, (2nd ed, Academic, New York, 1963), pp. 1741-1770.
34. A Kaniyoor, T Theres Baby, S Ramaprabhu, J. Mater. Chem., **20**, 8467 (2010).
35. J Luo,H Jang, J Huang , ACS Nano, **7**, 1464 (2013).
36. B. E. Warren, P. Bodestein, *Acta Cryst*, **18,** 282 (1965).
37. B. Saner, F. Okyay, Y. Yürüm, *Fuel* **89**, 1903 (2010).

38. B Saner, F Dinç, Y Yürüm *Fuel* **90**, 2609 (2011).
39. G. Srinivas, Y Zhu, R Piner, N Skipper, M Ellerby, R.Ruoff, *Carbon*, **48** 630 (2010).
40. S Chandra, S Sahu., P Pramanik, *Materials Science and Engineering B*, **167,** 133 (2010).
41. W. Chen, L. Yan, P.R. Bangal, *Carbon*, **48,** 1146 (2010).
42. L. M. Malard, M.A. Pimenta, G Dresselhaus, M.S. Dresselhaus, *Physics Reports*, **473**, 51 (2009).
43. J. C. Meyer, A. C. Ferrari, V. Scardaci, C. Casiraghi, M. Lazzeri, F. Mauri, S. Piscanec, D. Jiang, K.S. Novoselov, S. Roth, A.K. Geim, *Physical Review Letters*, **97**, 187401(2006).
44. A C. Ferrari, *Solid State Communications*, **143** 47 (2007).
45. V. Sridhar, J.H. Jeon, I.K. Oh, *Carbon*, **48**, 2953 (2010).
46. S. Stankovich, D.A. Dikin, R.D. Piner, K.A. Kohlhaas, A. Kleinhammes, Y. Jia, Y. Wu,S.T Nguyen, S.R. Rodney, *Carbon*, **45**, 1558 (2007).
47. Y. Ogawa, A. Nakamura, A. Tanaka, J. Temmyo, *Japanese Journal of Applied Physics*, **48**, 04C140 (2009).
48. F. Tuinstra, J.K. Koenig, *J. Chem. Phys.*, **53**, 1126 (1970).
49. XY Qi, D Yan, YK Jiang, Z Cao, ZZ Yu, F. Yavari, N Koratkar, *ACS Appl Mater Interfaces.* **3,** 3130 (2011)
50. A. *Dehé*, K. Fricke, K. Mutamba, H.L. Hartnagel, *J. Micromech*. Microeng. ***5*** *139 (1995)*.
51. *J Shojaii, K-Y Ng, MA Schmidt, J. Micromech. Systems;* **1**, 89 *(1992).*
52. H Lv, C Jiang, Z Xiang, B Ma, J Deng, W, *Flow Meas. Instr.* **30**, 66 (2013).

Table I- Sample description and synthesis parameters for GO and GN.

Sample number	*Initial Material*	*Drying Method*	*Specification and details*
GO1 , GO2	Graphite particle	-	Primary Hummer method
GO3, GO4	Graphite particle	-	Modified Hummer method
GO5 , GO6	Graphite flake	-	Modified Hummer method
GN1	GO1	Filter	Hydrazination
GN2, GN3	GO1	V*	Hydrazination
GN4	GO2	V	Hydrazination
GN5	GO3	V	Hydrazination
GN6	GO3	F*	Hydrazination
GN7	GO5	V	Hydrazination
GN9	GO6	F	Hydrazination

* Vacuum drying (V) and Freeze drying (F)

Table II: Details of the prepared graphene-polystyrene composites with different weight percentages of graphene nanosheets (GNs). The tick mark indicates the samples tested successfully.

Graphene (GN) content (wt. %)		0.0	0.5	1	2
GN5	Graphene sheets obtained from oxidized graphite particles using the modified Hummers method in vacuum drier	✓	✓	✓	✓
GN6	Graphene sheets obtained from oxidized graphite particles using the modified Hummers method in freeze drier	N/A	✓	✓	✓
GN7	Graphene sheets obtained from oxidized graphite flakes using the modified Hummers method in vacuum drier	N/A	✓	✓	✓
GN9	Graphene sheets obtained from oxidized graphite flakes using the modified Hummers method in freeze drier	N/A	✓	✓	✓

Table III- Data extracted from XRD patterns of different materials. d_{002} is the interatomic distance along c-axis, Lc is the parallel layer group dimension normal to the layers and L_a is lateral size of the graphene sheets.

	2θ(°)	*d_{002}(Å)*	*L_c(Å)*	*L_a(nm)*	Details
Graphite powder	26.53	3.36	-	-	-
Graphite flake	26.66	3.34	-	-	-
GO2	12.27	7.21	-	-	oxidized graphene exfoliated from graphite particles using the primary Hummer method
GO3	12.27	7.17	-	-	oxidized graphene exfoliated from graphite particles using the modified Hummer method
GO4	12.09	7.32	-	-	oxidized graphene exfoliated from graphite particles using the modified Hummer method
GN5	23.22	3.82	8.0	4.2	Graphene sheets obtained from oxidized graphite particles using the modified Hummers method in vacuum drier
GN6	23.56	4.08	6.0	22.2	Graphene sheets obtained from oxidized graphite particles using the modified Hummers method in freeze drier
GN7	23.45	5.90	6.0	29.6	Graphene sheets obtained from oxidized graphite flakes using the modified Hummers method in vacuum drier
GN9	23.22	6.11	5.0	12.2	Graphene sheets obtained from oxidized graphite flakes using the modified Hummers method in freeze drier

Table IV-Data calculated from Raman spectra of graphene nanosheets to infer the number of monolayers and size of GN sheets.

	I_D/I_G	$L_a(nm)$	W_G	Details
GN5	1.2790	3.4401	38.29	Graphene sheets obtained from oxidized graphite particles using the modified Hummers method in vacuum drier
GN6	1.2121	3.6300	45.23	Graphene sheets obtained from oxidized graphite particles using the modified Hummers method in freeze drier
GN7	0.8043	5.6705	30.11	Graphene sheets obtained from oxidized graphite flakes using the modified Hummers method in vacuum drier
GN9	0.7324	6.0076	28.37	Graphene sheets obtained from oxidized graphite flakes using the modified Hummers method in freeze drier

Figure Captions

Figure 1 Colloidal suspension of graphene oxide nanoparticles prepared according to the (a) Hummer and (b) modified Hummer method. (c) Dry powder of graphene nanosheets obtained after reduction and freeze drying of the modified Hummer solution.

Figure 2 XRD spectra of a) Graphite particles prior to oxidization, b) oxidized graphene exfoliated from graphite particles using the primary Hummer method (GO1,GO2), c) oxidized graphene exfoliated from graphite particles using the modified Hummer method (GO3,GO4), (d) oxidized graphene exfoliated from graphite flakes using the modified Hummer method (GO5, GO6); (Note: panel (a) is plotted in logarithmic scale for clarity.).

Figure 3 XRD patterns of graphene nanosheets for samples (a) Graphene sheets obtained from oxidized graphite particles using the modified Hummers method in vacuum drier; GN5, (b) Graphene sheets obtained from oxidized graphite particles using the modified Hummers method in freeze drier; GN6, (c) Graphene sheets obtained from oxidized graphite flakes using the modified Hummers method in vacuum drier ; GN7 and (d) Graphene sheets obtained from oxidized graphite flakes using the modified Hummers method in freeze drier; GN9. Insets show SEM images of the corresponding structures.

Figure 4 FTIR spectra of (a) GO3: oxidized graphene exfoliated from graphite particles using the modified Hummer method, (b) GO4: oxidized graphene exfoliated from graphite particles using the modified Hummer method, (c) GN5: Graphene sheets obtained from oxidized graphite particles using the modified Hummers method in vacuum drier and (d) GN9: Graphene sheets obtained from oxidized graphite flakes using the modified Hummers method in freeze drier.

Figure 5 Raman Spectra of (a) Graphene sheets obtained from oxidized graphite particles using the modified Hummers method in vacuum drier; GN5, (b) Graphene sheets obtained from oxidized graphite particles using the modified Hummers method in freeze drier; GN6, Graphene sheets obtained from oxidized graphite flakes using the modified Hummers method in vacuum drier; GN7 and Graphene sheets obtained from oxidized graphite flakes using the modified Hummers method in freeze drier; GN9.

Figure 6: Dimensions parameters calculated by Raman spectra of graphene nanosheets to infer the number of monolayers and size of GN sheets.

Figure 7 A typical (a) SEM image and (b) piezoresistivity plot of GN/PS composites produced by in-situ emulsion polymerization of styrene in the presence of graphene,

Figure 8 Electrical conductivity of GN/PS composites as a function of GN content: a) GN5, b) GN6, c) GN7 and d) GN9.

Figure 9: Pressure sensor array.
The sensor head (lower part of panel (a)) is imprinted with a spatial pressure profile in the form of the "copyright" symbol. The Composite array senses the pressure profile and outputs a binary profile on the computer screen at the back. Panel (b): detail of the 8x8 composite array used to sense pressure. Each element is addressed by the field effect transistor at the back of the printed circuit board.

Figure 1
Click here to download Figure: Fig 1.tif

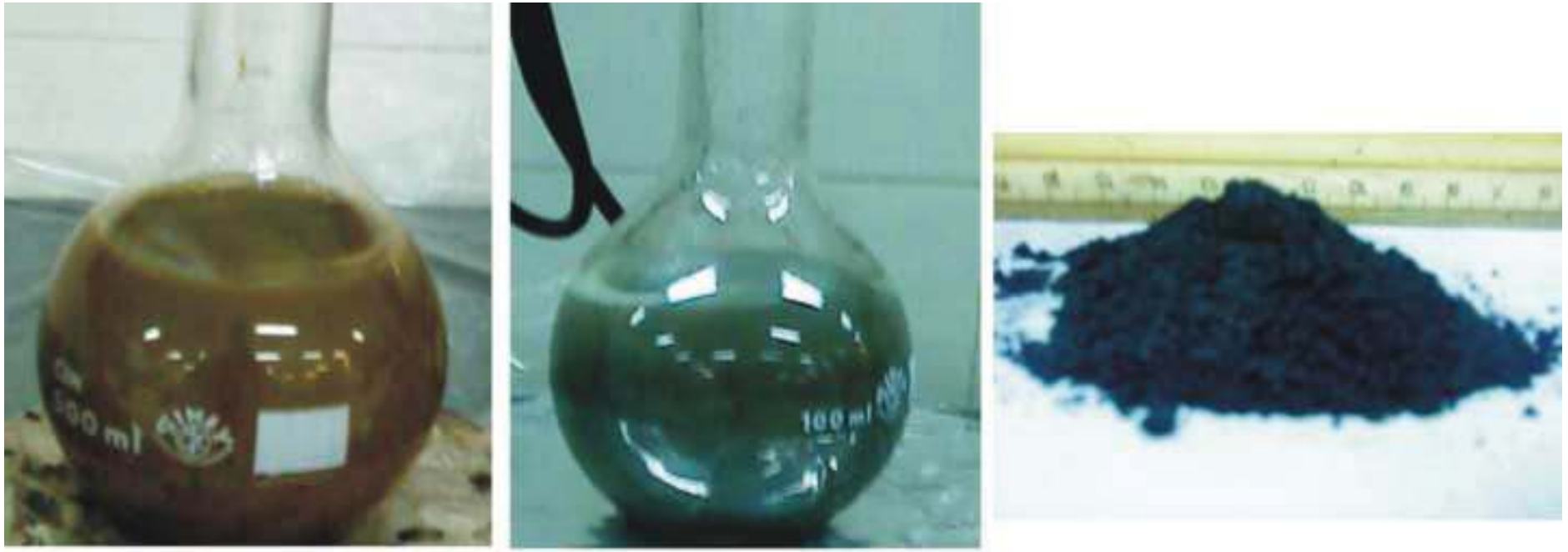

Figure 2
Click here to download Figure: Fig 2.TIF

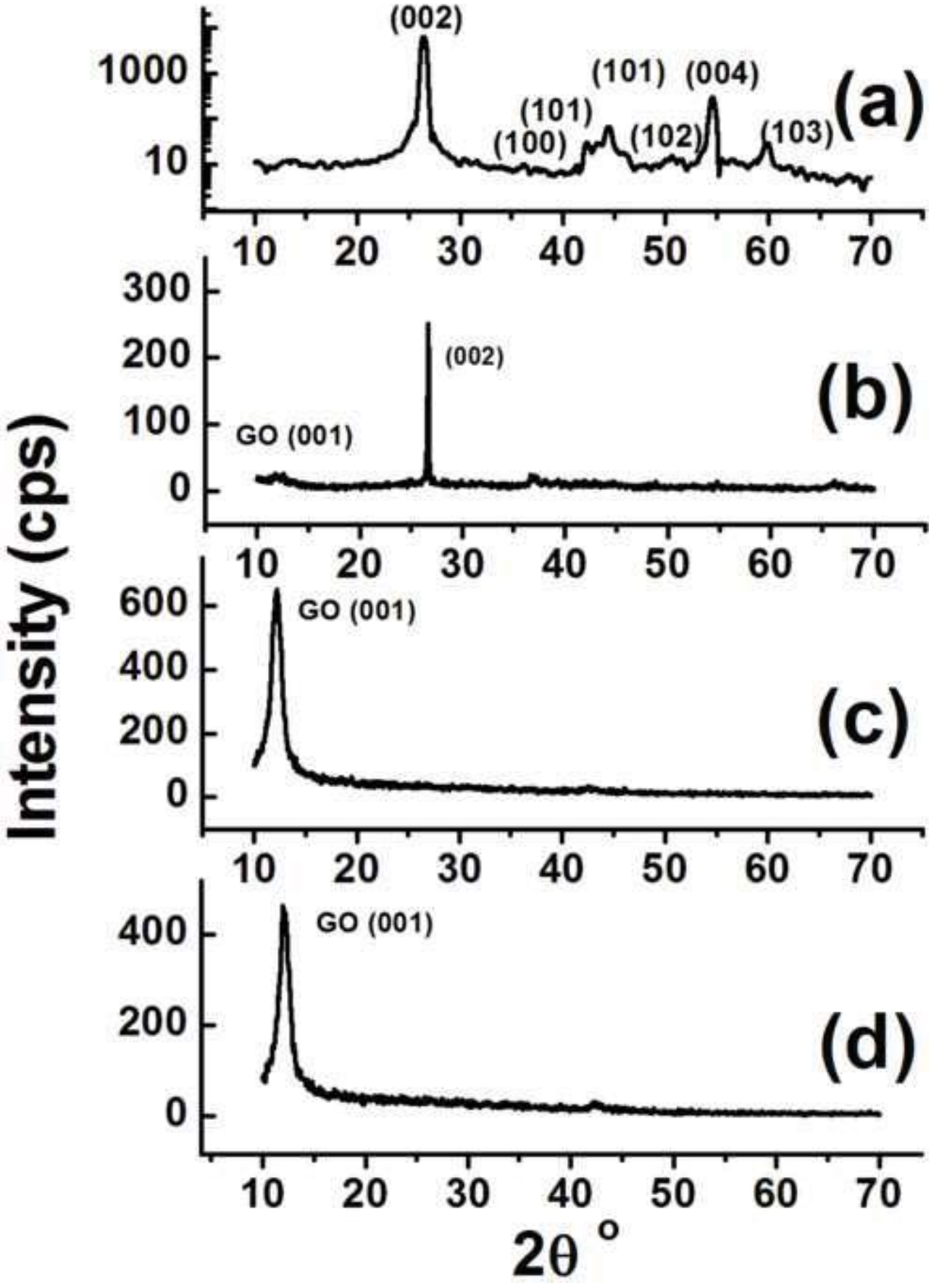

Figure 2 EPS
Click here to download Figure: Figure 2.EPS

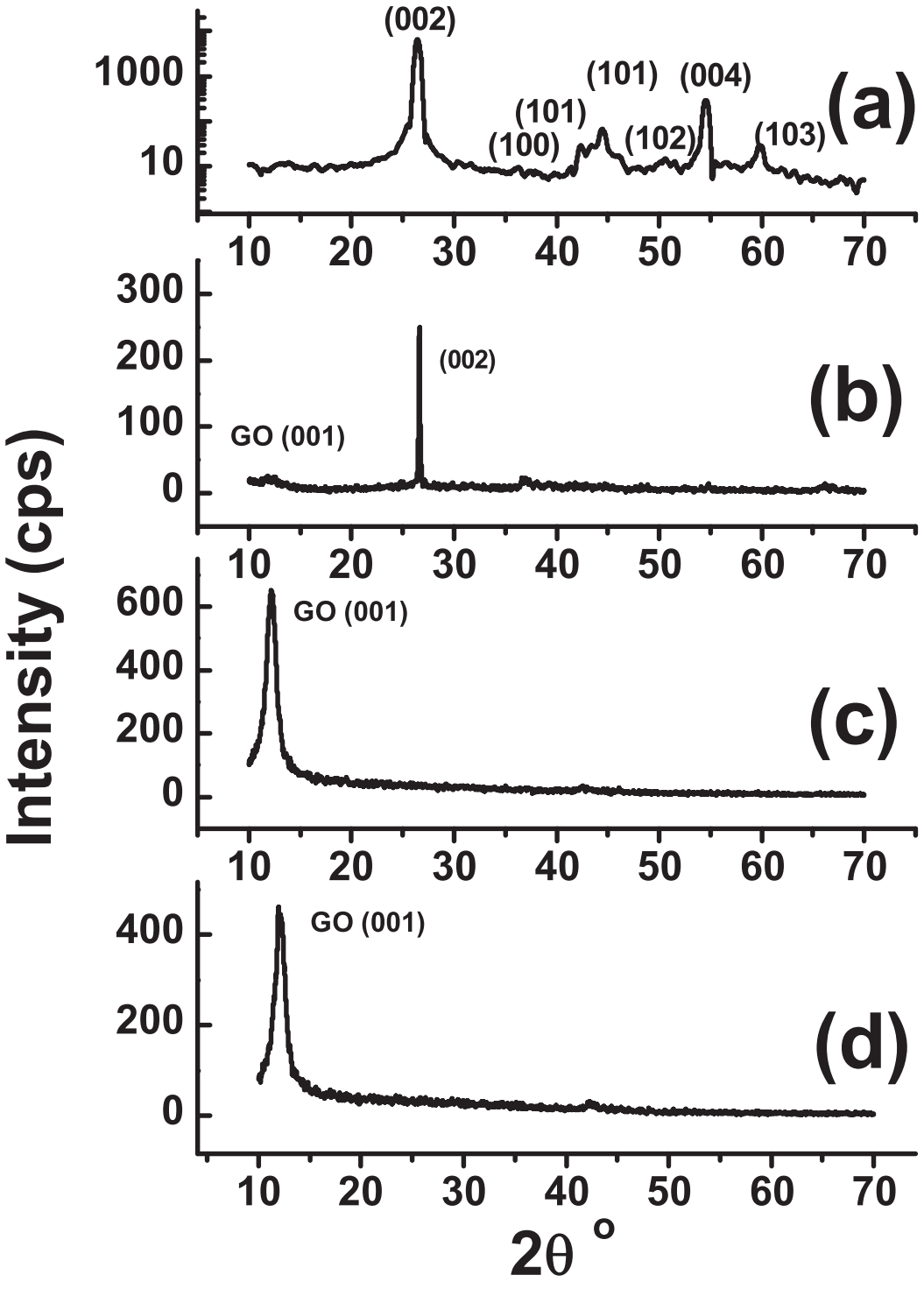

Figure 3
Click here to download Figure: Fig 3.TIF

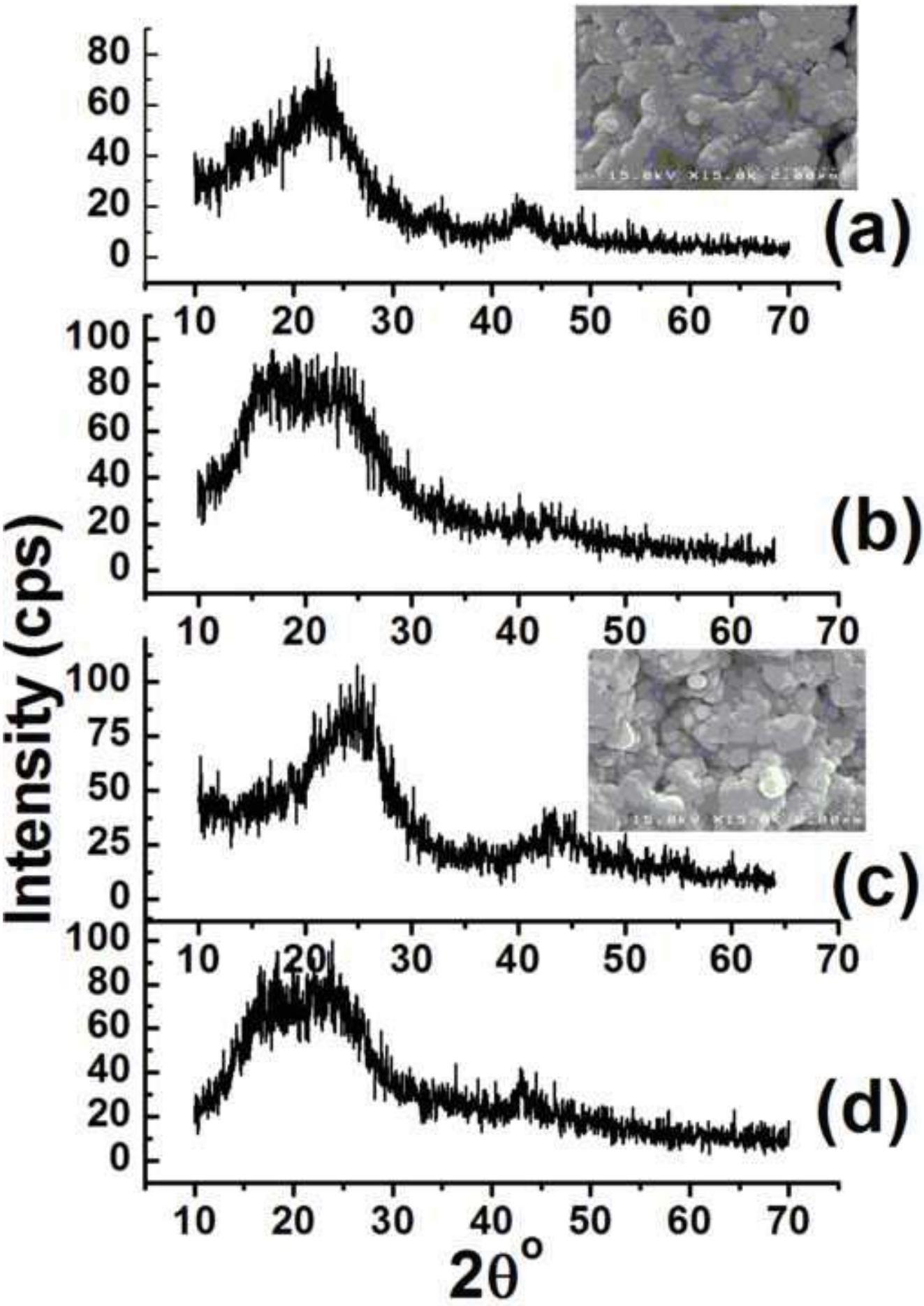

Figure 3 EPS
Click here to download Figure: Fig 3 EPS.EPS

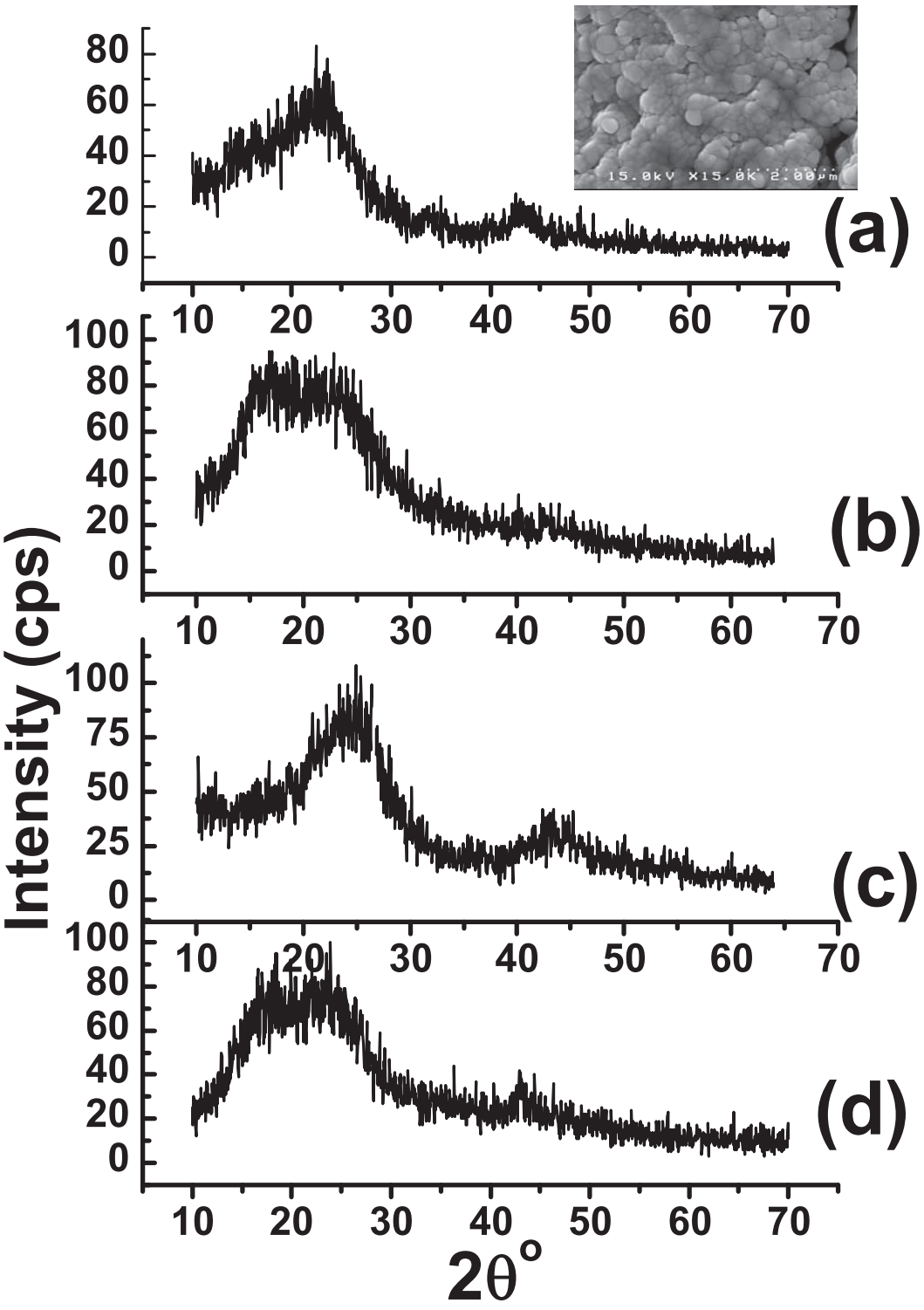

Figure 4
Click here to download Figure: Fig 4.tif

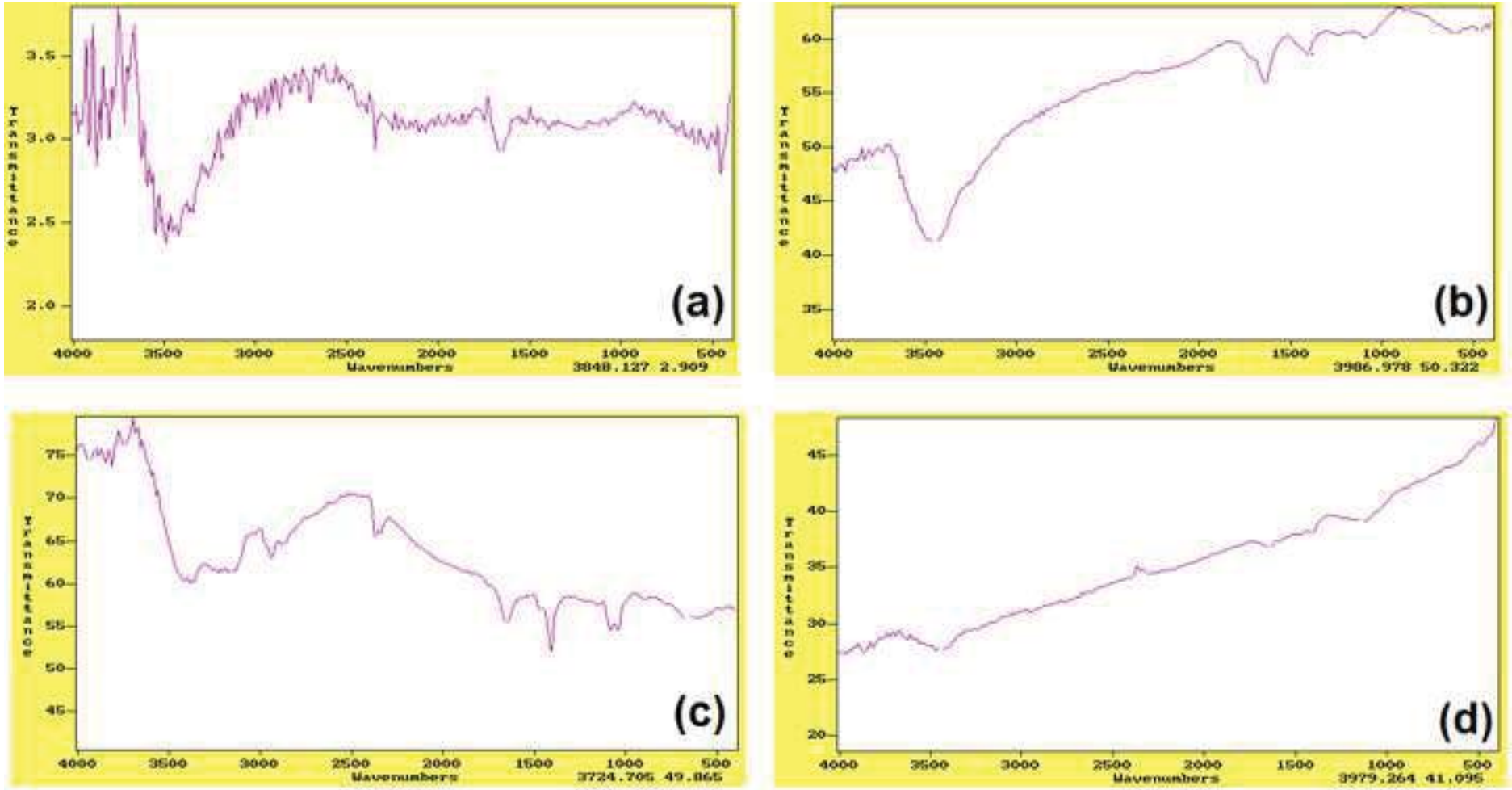

Figure 5
Click here to download Figure: Fig 5.TIF

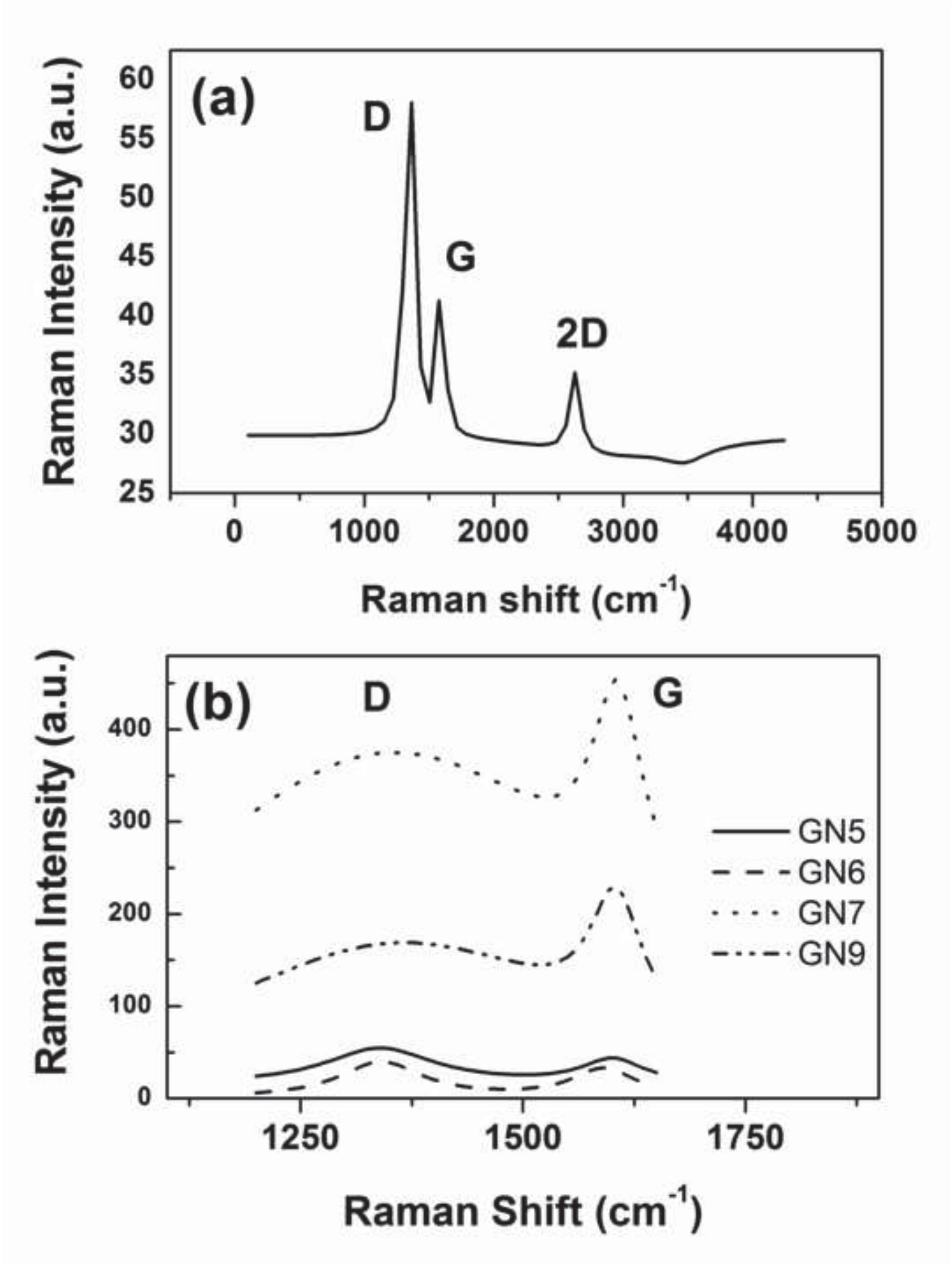

Figure 5 EPS
Click here to download Figure: Fig 5 eps.EPS

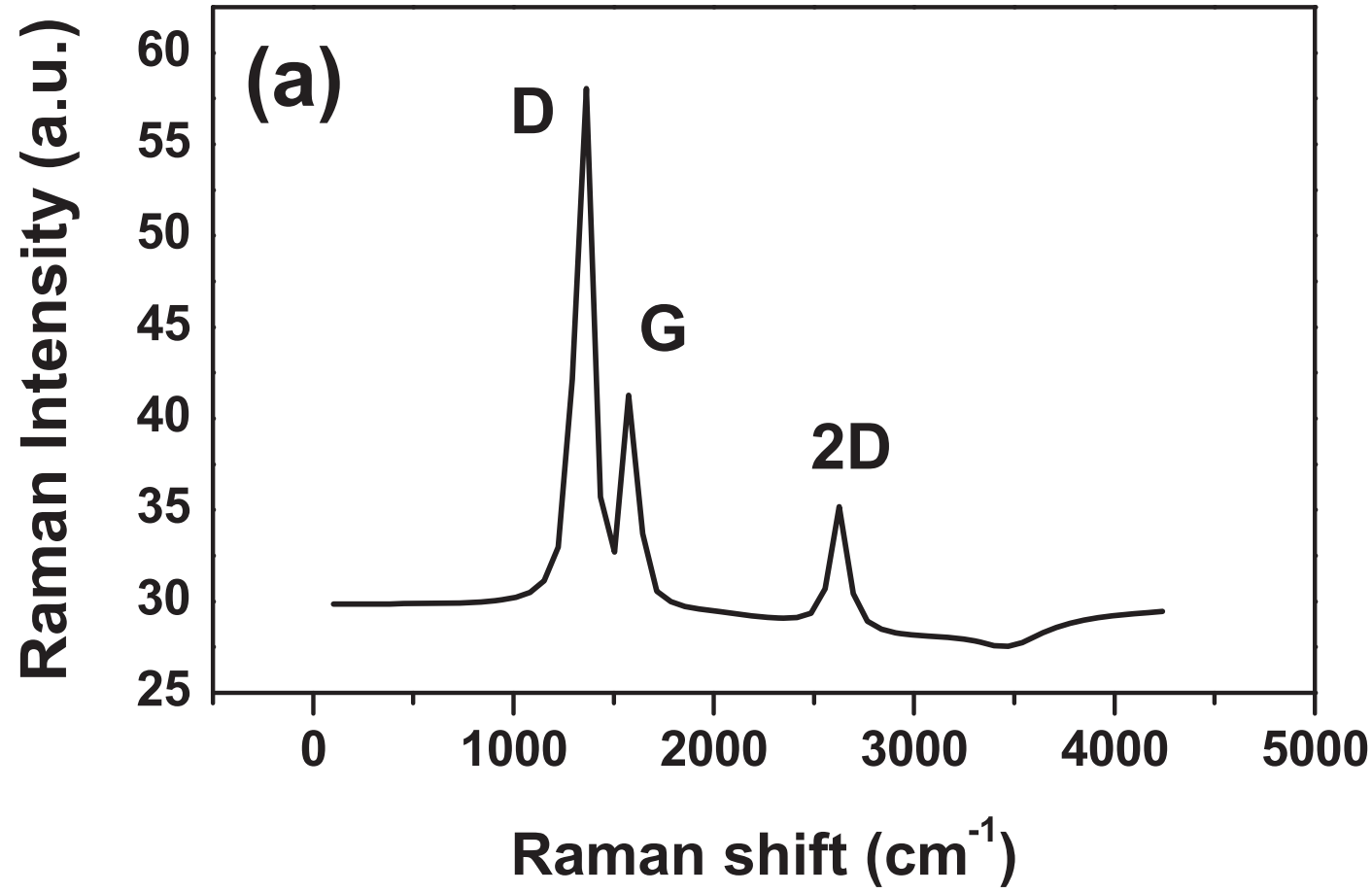

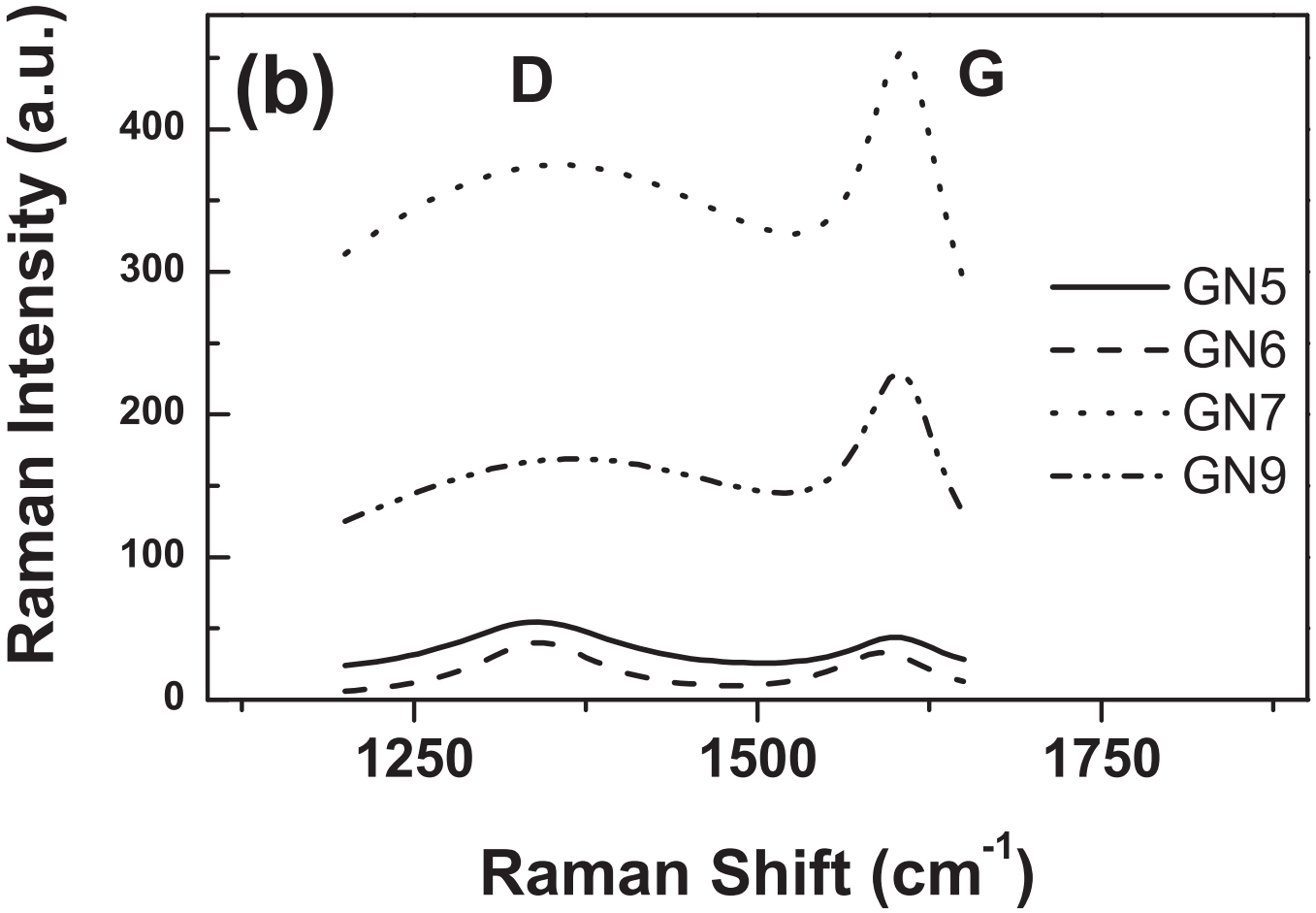

Figure 6
Click here to download Figure: Fig 6.TIF

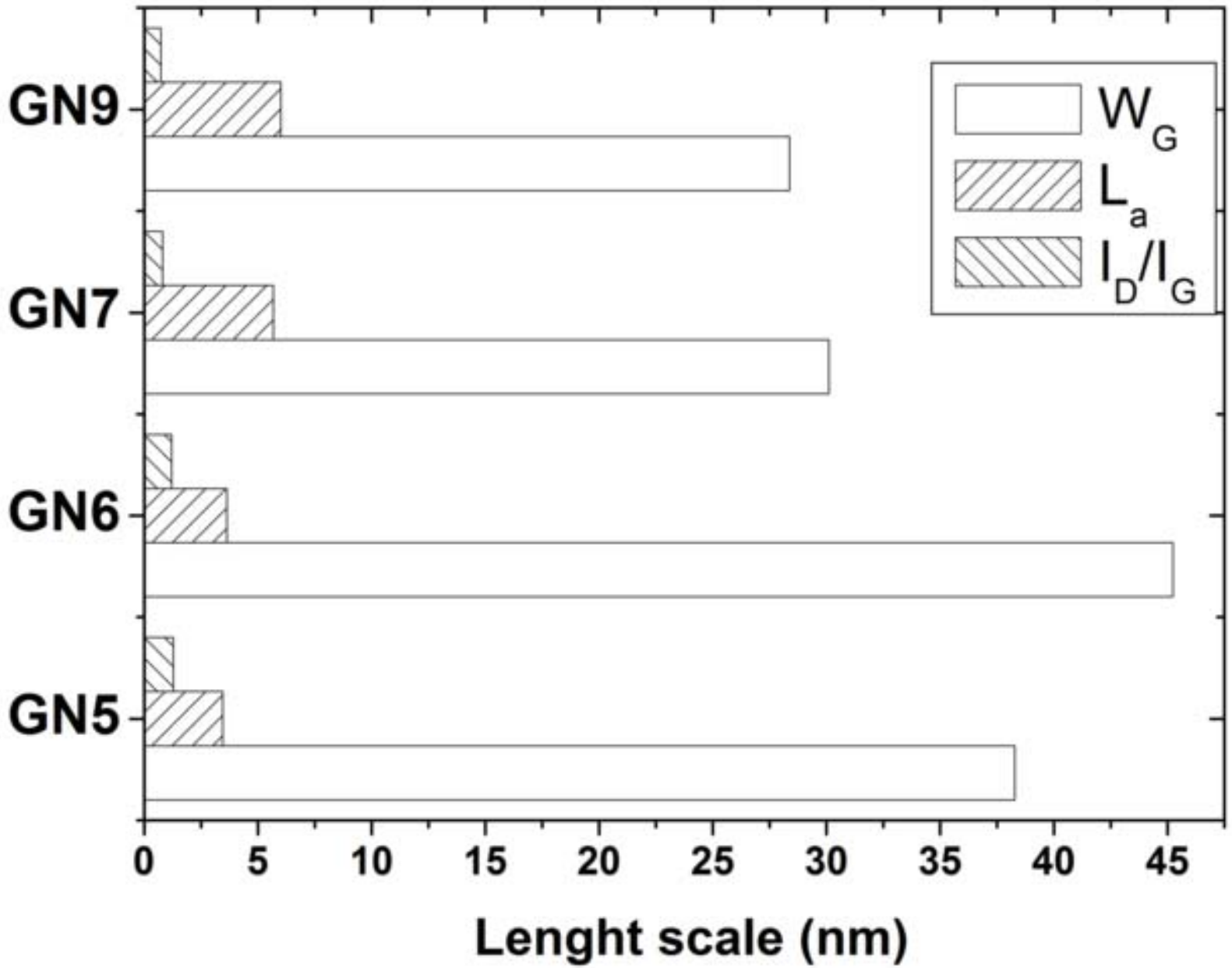

Figure 6 EPS
Click here to download Figure: Figure 6.EPS

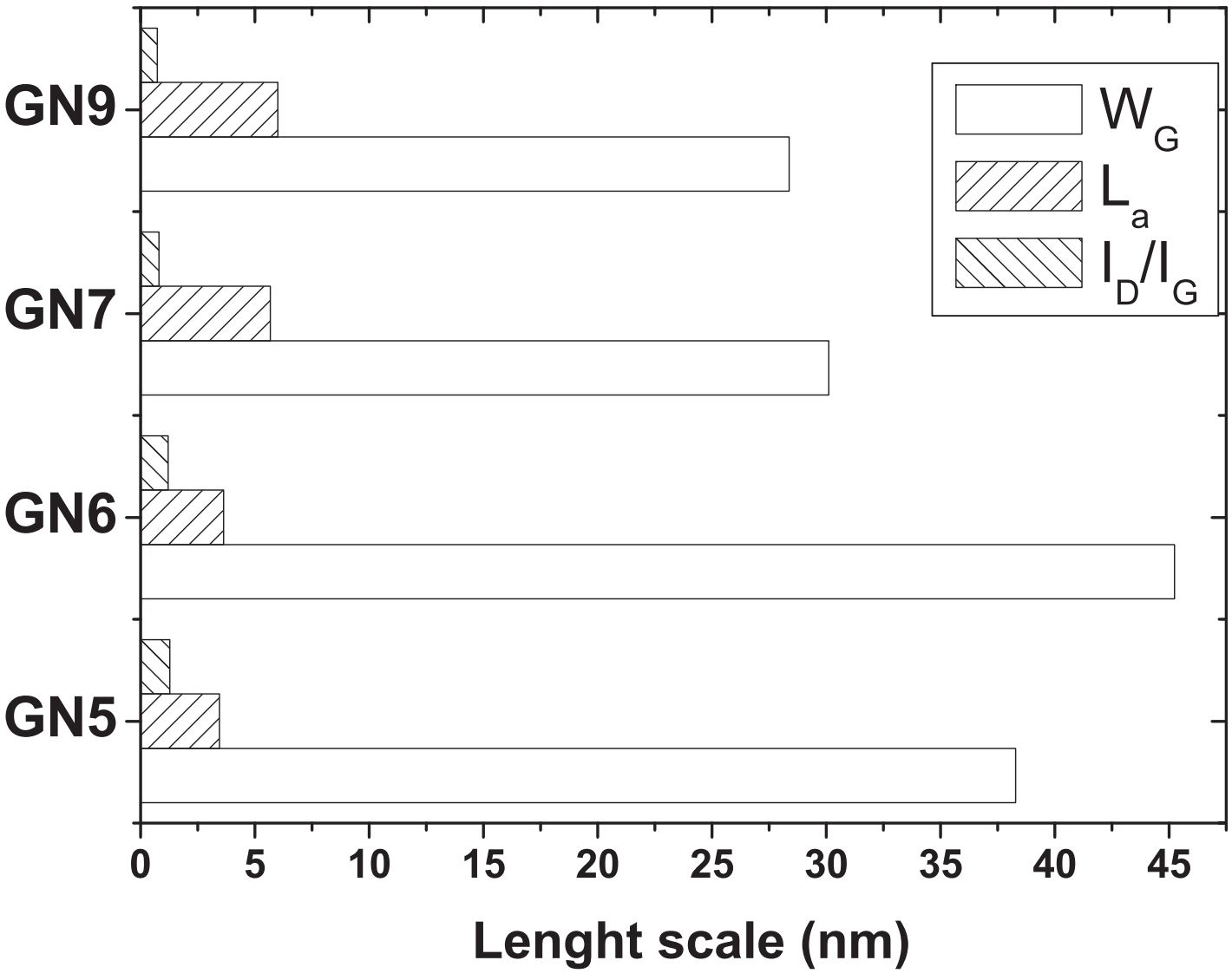

Figure 7a
Click here to download Figure: Fig 7a.tif

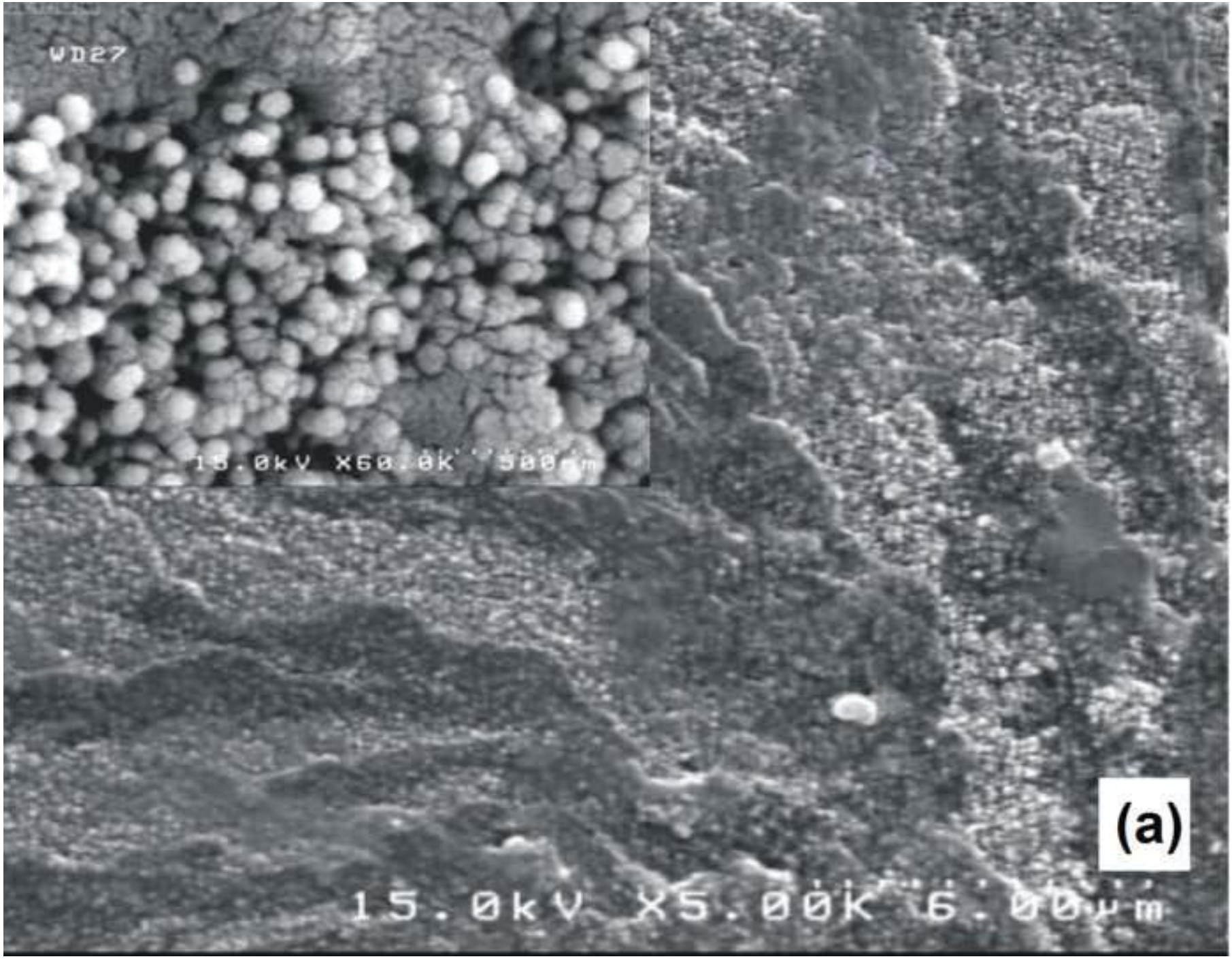

Figure 7b
Click here to download Figure: Fig 7b.TIF

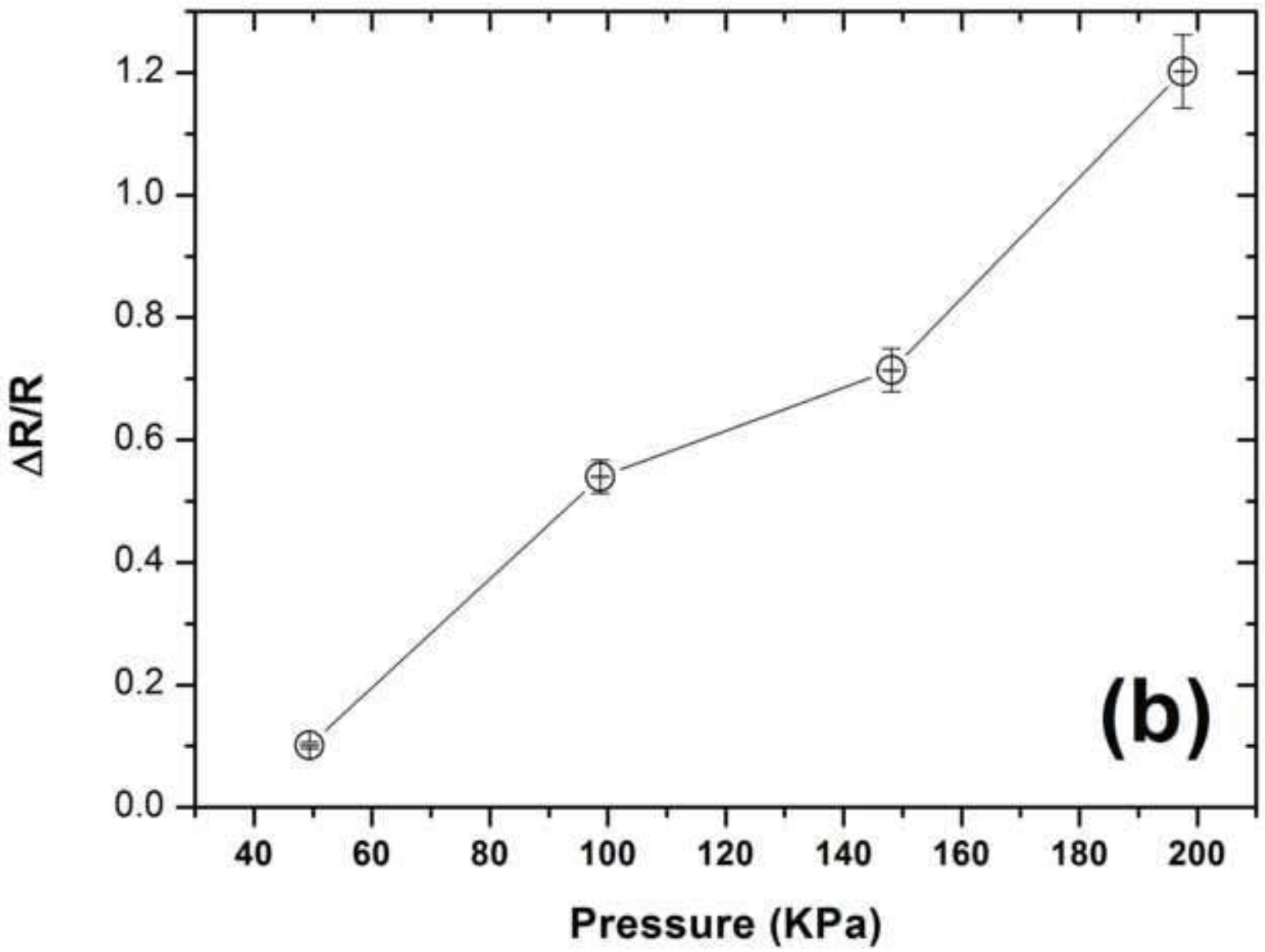

Figure 7b EPS
Click here to download Figure: Figure 7b.EPS

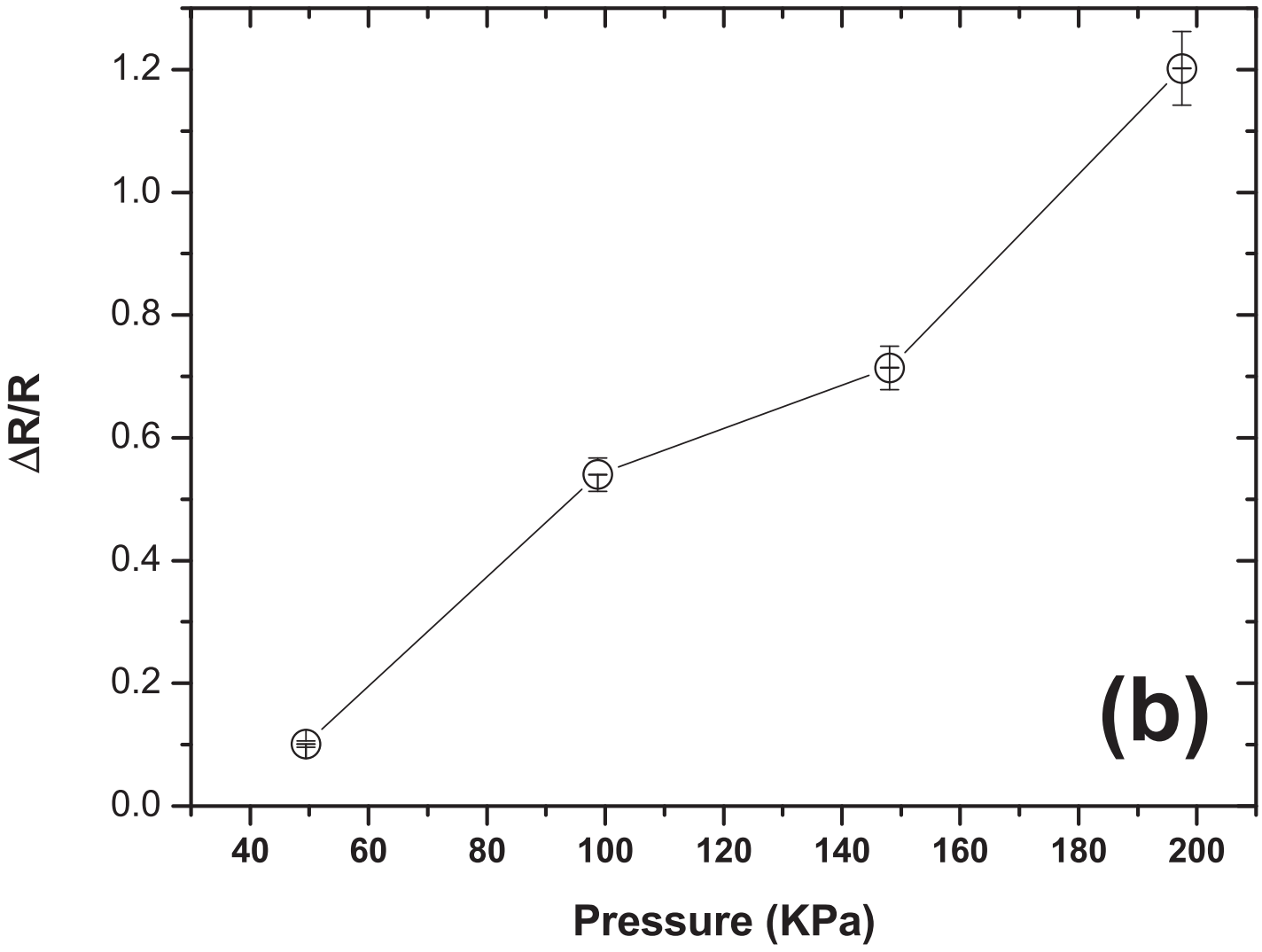

Figure 8
Click here to download Figure: Fig 8.TIF

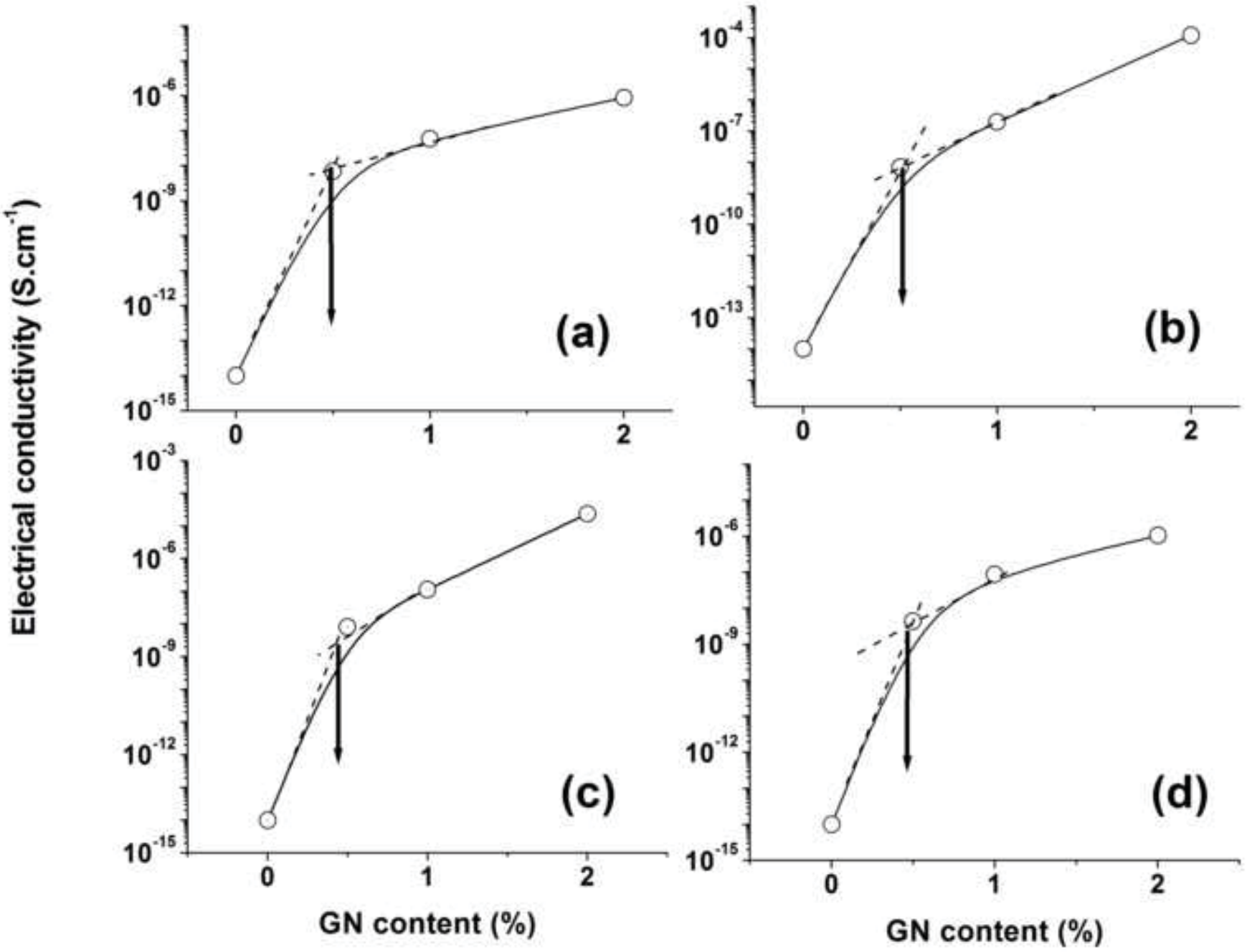

Figure 8 EPS
Click here to download Figure: Figure 8.EPS

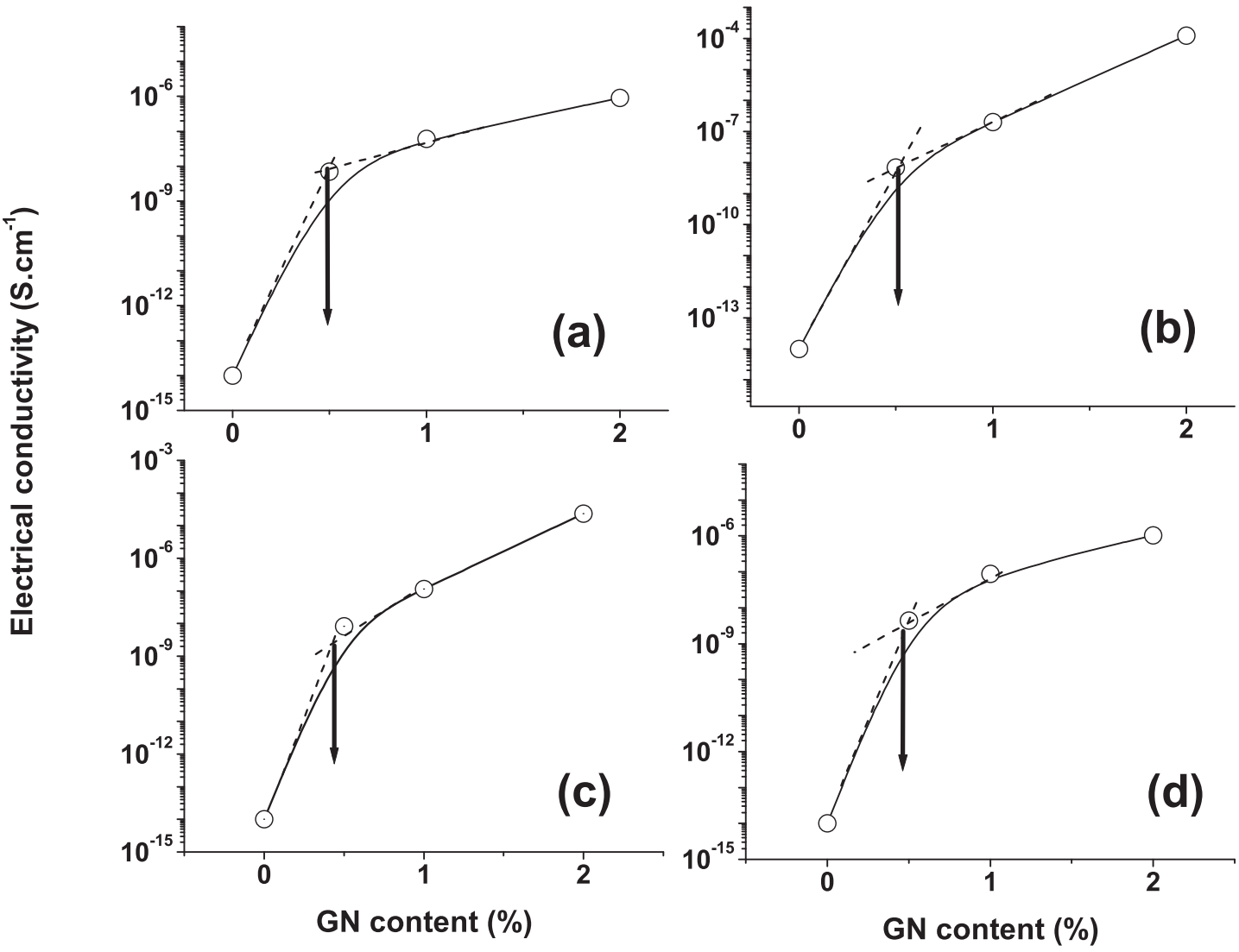

Figure 9
Click here to download Figure: Fig9.tif